Supplemental Material

Elastocapillary crease

Qihan Liu[1]*, Tetsu Ouchi[2]*, Lihua Jin[3], Ryan Hayward[2]†, Zhigang Suo[1]‡

[1]School of Engineering and Applied Sciences, Kavli Institute for Bionano Science and Technology, Harvard University, Cambridge, MA, 02138, USA

[2]Department of Polymer Science & Engineering, University of Massachusetts, Amherst, MA, 01003, USA

[3]Department of Mechanical and Aerospace Engineering, University of California, Los Angeles, CA 90095, USA

* These authors contributed equally to this work

† rhayward@mail.pse.umass.edu

‡ suo@seas.harvard.edu

Continuum theory of elastocapillarity

The continuum theory of elastocapillarity has been reviewed recently [1]. Here we list the key equations related to our work. Consider a body in three dimensions. When the body is in the reference state, a material particle occupies a place of coordinate $\mathbf{X}$. When the body deforms to the current state, and the material particle $\mathbf{X}$ moves to a place of coordinate $\mathbf{x}$. The deformation of the body is described by the map

$$\mathbf{x} = \mathbf{x}\left(\mathbf{X}\right). \tag{1}$$

The domain of this function is the coordinates of material particles when the body is in the reference state. The range of this function is the coordinates of the places occupied by the material particles. Define the deformation gradient by

$$F_{iK} = \frac{\partial x_i(\mathbf{X})}{\partial X_K}. \tag{2}$$

The free energy of the body is

$$\int W(\mathbf{F}) dV + \int \gamma(\mathbf{F}) da. \tag{3}$$

Here W is the free energy of the bulk material per unit reference volume, dV is a volume element in the reference state, γ is the interfacial energy per unit current area, and da is an area element in the current state. The free energy per unit volume is a function of the deformation gradient, $W(\mathbf{F})$. In general, the interfacial energy per unit area is also a function of the deformation gradient, $\gamma(\mathbf{F})$.

For a pure liquid in contact with gas, when a new surface area is created, molecules from the bulk merge onto the surface. The structure and composition of the surface remain the same. As a result, γ is a constant independent of the deformation. For most gels the crosslink density is low so that individual chains largely preserve their configuration in a liquid state [2]. The liquid-like property has manifested itself in many different aspects, including the Neo-Hookean elasticity [3], the success of using Flory-Huggins solution model to predict the swelling of gel [4] and the liquid-like dielectric behavior in elastomers [5]. We thus expect the surface energy of a gel to have liquid-like behavior as well. In the following discussion, we will take γ as a constant independent of the deformation.

Consider a piece of hydrogel in air with applied surface traction. At equilibrium, the first order variation of the free energy of the whole system equals the applied work:

$$\int \delta W \, dV + \gamma \delta a = \int t_i \, \delta x_i \, da \, . \tag{4}$$

Here δa denotes the total variation of the interfacial area between hydrogel and air, and t_i is the traction per unit current area. For a continuous and smooth surface, the following geometric relation holds:

$$\delta a = \int K n_i \delta x_i da. \tag{5}$$

Here K is the mean curvature:

$$K = \frac{1}{R_1} + \frac{1}{R_2}, \tag{6}$$

where R_1 and R_2 are the principal radii of curvature of the surface in the current state. The surface between hydrogel and air may not be continuous with respect to surface of the hydrogel if there is self-contact. The surface may not be smooth if there is a triple junction. Here we assume none of those situations happen.

Recall that the nominal stress and deformation gradient are work-conjugate,

$$\delta W = s_{iK} \delta F_{iK} \, . \tag{7}$$

The nominal stress relate to the true stress as

$$\sigma_{ij} = s_{iK} F_{jK} / J \, . \tag{8}$$

The deformation maps an element of material area dA in the reference state to an element da in the current state. The two areas are related as

$$F_{iK} n_i da = J N_K dA \, . \tag{9}$$

We write

$$\begin{aligned}
&\int \delta W dV = \int s_{iK}\delta F_{iK} dV = \int s_{iK}\delta x_{i,K} dV \\
&= \int \left[\left(s_{iK}\delta x_i \right)_{,K} - s_{iK,K}\delta x_i \right] dV \\
&= \int s_{iK} N_K \delta x_i dA - \int s_{iK,K}\delta x_i dV \\
&= \int \sigma_{ij} n_j \delta x_i da - \int s_{iK,K}\delta x_i dV
\end{aligned} \tag{10}$$

A combination of the above equations gives that

$$-\int s_{iK,K}\delta x_i dV + \int \left[\left(\sigma_{ij} + \gamma K \delta_{ij} \right) n_j - t_i \right] \delta x_i da = 0. \tag{11}$$

The condition of equilibrium holds for arbitrary small changes of the field of deformation, δx_i. Consequently, the above condition of equilibrium is equivalent to

$$s_{iK,K} = 0 \tag{12}$$

in the interior of the body, and

$$\left(\sigma_{ij} + \gamma K \delta_{ij} \right) n_j = t_i \tag{13}$$

on the surface of the body.

Linear perturbation analysis

Linear perturbation analysis of elastocapillary wrinkles has been conducted in [6]. Here we adapt the analysis to a material under generalized plane strain condition. We assume that the deswelling of the hydrogel during the experiment is negligible, and model the hydrogel as an incompressible Neo-Hookean material. The free energy of the material per reference volume is:

$$W\left(\mathbf{F} \right) = \frac{\mu}{2} F_{iK} F_{iK}, \tag{14}$$

where μ is the shear modulus. The nominal stress is:

$$s_{iK} = \mu F_{iK} - \Pi H_{iK}, \tag{15}$$

where

$$H_{iK} = \partial \det(\mathbf{F}) / \partial F_{iK}. \tag{16}$$

The quantity Π is the Lagrange multiplier to ensure incompressibility. The variation of the stress is:

$$\delta s_{iK} = \mu \delta F_{iK} - \delta \Pi H_{iK} + \Pi H_{iJ} H_{lK} \delta F_{lJ} \tag{17}$$

The force balance requires that

$$\delta s_{pQ,Q} = 0. \tag{18}$$

The incompressibility requires that

$$H_{iK} \delta F_{iK} = 0 \tag{19}$$

(18) and (19) constitute a complete set of equations for $\delta \mathbf{x}, \delta \Pi$.

Consider a block of hydrogel bounded on the substrate (Fig.S1). At the free surface ($X_2 = 0$), the tangent traction should vanish. The normal traction should equate the Laplace pressure γK.

$$\begin{cases} \delta \sigma_{\mathbf{tn}} = 0 \\ \delta \sigma_{\mathbf{nn}} = \gamma \mathbf{n} \cdot \delta \mathbf{x}_{,\mathbf{tt}} \end{cases}. \tag{20}$$

At the bounded surface ($X_2 = H$), the perturbed displacement should vanish:

$$\begin{cases} \delta x_1 = 0 \\ \delta x_2 = 0 \end{cases} \tag{21}$$

(18-21) constitutes a complete boundary value problem which a valid perturbation field should satisfy.

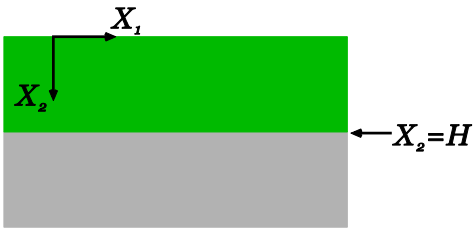

Fig.S1. Consider a piece of elastomer compressed under generalized plane strain condition. The hydrogel has a free surface on one side and is bounded at the other side. Set up a Cartesian reference system with X_1 along the surface of the hydrogel and X_2 pointing from the free surface towards the bounded surface. The bounded surface locates at $X_2 = H$, where H is the thickness of the hydrogel in the reference configuration.

Consider the generalized plane strain condition with unperturbed deformation gradient

$$\mathbf{F} = \begin{bmatrix} \lambda_1 & & \\ & (\lambda_1\lambda_3)^{-1} & \\ & & \lambda_3 \end{bmatrix} \tag{22}$$

and assume the perturbed field to be

$$\delta\mathbf{F} = \begin{bmatrix} \delta x_{1,1} & \delta x_{1,2} & \\ \delta x_{2,1} & \delta x_{2,2} & \\ & & 0 \end{bmatrix}. \tag{23}$$

The variation of the stress under these assumptions is

$$\begin{cases} \delta s_{11} = \mu\left(1+\lambda_1^{-4}\lambda_3^{-2}\right)\delta x_{1,1} - \delta\Pi\left(\lambda_1\right)^{-1} \\ \delta s_{12} = \mu\delta x_{1,2} + \mu\lambda_1^{-2}\lambda_3^{-1}\delta x_{2,1} \\ \delta s_{21} = \mu\delta x_{2,1} + \mu\lambda_1^{-2}\lambda_3^{-1}\delta x_{1,2} \\ \delta s_{22} = 2\mu\delta x_{2,2} - \delta\Pi\lambda_1\lambda_3 \end{cases} \tag{24}$$

with the rest of the stress components vanish. Assume

$$\begin{cases} \delta x_1 = A\exp\left(kX_2\right)\cos\omega X_1 \\ \delta x_2 = B\exp\left(kX_2\right)\sin\omega X_1 \\ \delta\Pi = C\exp\left(kX_2\right)\sin\omega X_1 \end{cases} \tag{25}$$

Inserting into the governing equations (18) and (19) we have

$$\begin{bmatrix} \mu k^2 - \mu\left(1+\dfrac{1}{\lambda_1^4\lambda_3^2}\right)\omega^2 & \dfrac{\mu\omega k}{\lambda_1^2\lambda_3} & -\dfrac{\omega}{\lambda_1} \\ -\dfrac{\mu\omega k}{\lambda_1^2\lambda_3} & 2\mu k^2 - \mu\omega^2 & -\lambda_1\lambda_3 k \\ -\dfrac{\omega}{\lambda_1} & \lambda_1\lambda_3 k & 0 \end{bmatrix} \begin{bmatrix} A \\ B \\ C \end{bmatrix} = 0 \tag{26}$$

To have non-trivial solution we require the determinant of the coefficient matrix to vanish, which gives:

$$\lambda_1^4\lambda_3^2 k^4 - \left(1+\lambda_1^4\lambda_3^2\right)\omega^2 k^2 + \omega^4 = 0. \tag{27}$$

The roots are $k_1 = \omega, k_2 = -\omega, k_3 = \dfrac{\omega}{\lambda_1^2\lambda_3}, k_4 = -\dfrac{\omega}{\lambda_1^2\lambda_3}$. So the general solution can be expressed in the following form:

$$\begin{bmatrix} \delta x_1 & \delta x_2 & \delta\Pi \end{bmatrix} = \begin{bmatrix} \cos\omega X_1 & \sin\omega X_1 & \sin\omega X_1 \end{bmatrix} \begin{bmatrix} \sum_i A_i \exp\left(k_i X_2\right) \\ \sum_i B_i \exp\left(k_i X_2\right) \\ \sum_i C_i \exp\left(k_i X_2\right) \end{bmatrix}. \tag{28}$$

The general solution need to satisfy the governing equations (18) and (19) at every point in the field. As a result, coefficients A_i, B_i, C_i are constrained by the following condition:

$$\begin{bmatrix} A_i \\ B_i \\ C_i \end{bmatrix} = B_i \begin{bmatrix} \dfrac{\lambda_1^2\lambda_3 k}{\omega_i} \\ 1 \\ \dfrac{\mu\left(k_i^2 - \omega^2\right)}{\lambda_1\lambda_3 k_i^2} \end{bmatrix} \tag{29}$$

Transform the boundary condition at $X_2 = 0$ (20) to the reference state:

$$\begin{cases} \delta s_{12} = 0 \\ \delta s_{22} = -\gamma \delta x_{2,11} \lambda_3 / \lambda_1 \end{cases} \tag{30}$$

Inserting (28) and (29) into (21) and (30), we have the following coefficient matrix:

$$\begin{bmatrix} \lambda_1^4\lambda_3^2+1 & \lambda_1^4\lambda_3^2+1 & 2 & 2 \\ 2-\dfrac{\lambda_3\gamma}{\lambda_1\mu H}\bar{\omega} & -2-\dfrac{\lambda_3\gamma}{\lambda_1\mu H}\bar{\omega} & \dfrac{\lambda_1^4\lambda_3^2+1}{\lambda_1^2\lambda_3}-\dfrac{\lambda_3\gamma}{\lambda_1\mu H}\bar{\omega} & -\dfrac{\lambda_1^4\lambda_3^2+1}{\lambda_1^2\lambda_3}-\dfrac{\lambda_3\gamma}{\lambda_1\mu H}\bar{\omega} \\ \lambda_1^2\lambda_3\exp(\bar{\omega}) & -\lambda_1^2\lambda_3\exp(-\bar{\omega}) & \exp\left(\dfrac{\bar{\omega}}{\lambda_1^2\lambda_3}\right) & -\exp\left(-\dfrac{\bar{\omega}}{\lambda_1^2\lambda_3}\right) \\ \exp(\bar{\omega}) & \exp(-\bar{\omega}) & \exp\left(\dfrac{\bar{\omega}}{\lambda_1^2\lambda_3}\right) & \exp\left(-\dfrac{\bar{\omega}}{\lambda_1^2\lambda_3}\right) \end{bmatrix}. \tag{31}$$

Here $\bar{\omega} = \omega H = 2\pi H / L$. To have non-trivial solution, the determinant of this matrix needs to vanish as well. Given λ_3, L, this determines the critical λ_2. For given values of $\gamma / \mu H$ and λ_3, there is a L with the maximum $\lambda_{2\max}$. The critical strain for wrinkle is defined as $\varepsilon_{wrinkle} = 1 - \lambda_{2\max}$.

Finite element method to compute the bifurcation diagram

Physically, interface is a thin layer of material of which the free energy density is different from the bulk. In finite element simulation, this could be represented by a layer of shell element tied to the boundary of the bulk material, with the material model of the shell element reflecting the free energy density of the surface.

In the case of constant surface tension γ, the effect of interfacial tension can be easily imitated by linear elastic shell, which is widely available in commercial finite element packages. To ensure that γ is independent of deformation, we require the stress and the cross section of the section both to be constant. That means, the shear

modulus, $\mu << \gamma$, and the Poisson's ratio $\nu = 0$. The finite value of the surface tension could be achieved by prescribe a finite residue stress.

We simulated the post-bifurcation behavior of our model system (the green part of Fig.S1) using commercial finite element software ABAQUS. The simulation is done under plane strain condition. A rectangular area of Neo-Hookean material is created to represent the sample. A layer of beam element is tied to the top boundary of the sample to imitate surface tension. The bottom of the sample is prescribed to be flat. A linear horizontal displacement field corresponding to the compression is applied. This imitates the effect of loading by a stiff substrate. For each value of the elastocapillary number $\gamma / \mu H$, the width of one half of the optimal wavelength for wrinkle is simulated. The left and right boundaries are prescribed to remain vertical. The material can slide up and down. The top-left corner of the sample is finely meshed so that the element size is at least one order of magnitude small than γ / μ.

During the simulation, the material is first compressed above the critical strain of wrinkle. Since the initial surface is perfectly flat, the bifurcation point will not cause any problem in the simulation. Then the top-left corner is pulled downward under displacement control. The displacement control is relaxed in the next step. The configuration is automatically relaxed towards the stable part of the post-bifurcation path. In the final step, the Riks method is used to track the post-buckling path all the way back to the bifurcation point [7]. Simulation result is summarized in Fig.S2.

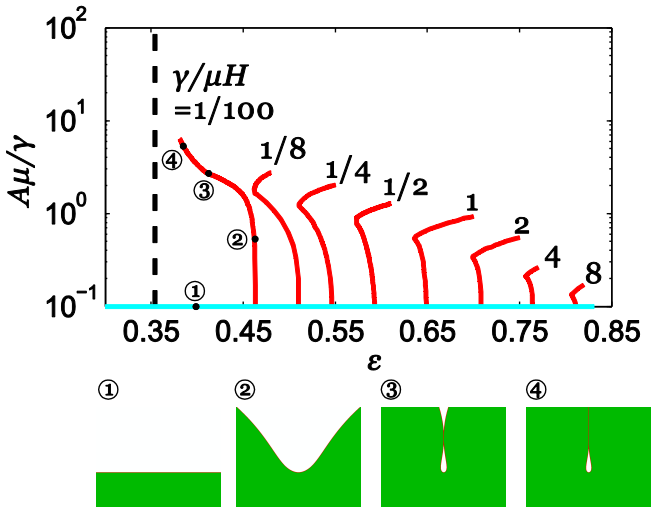

FIG.S2. The bifurcation diagrams simulated by finite element method. Red lines correspond to the bifurcation diagrams at different $\gamma/\mu H$ values. The dotted line is the critical strain for crease without elastocapillary effect. The inlets are the simulated deformation near the crease tip at different stages on the loading path.

Finite element simulation of ε_c when $\gamma_{con}=0$

In the $\gamma_{con}=0$ model, the original surface is divided into two regions in the crease state: the surface tension free region in the crease and the constant surface tension region outside the crease. The free energy of a creased film like this has the form: $W\left(\gamma/\mu H, l_c/H, \varepsilon\right)$. Here l_c is the contact length of the crease. At equilibrium,

$\delta W/\delta l_c=0$. Using finite element method, we build a model for each given $\gamma/\mu H$ and l_c/H, Fig.S3a. $W\left(\gamma/\mu H, l_c/H, \varepsilon\right)$ is calculated by compressing the model for a range of ε. For any point on the bifurcation diagram, the free energy of two models with $\delta l_c=0.005H$ is compared. The point of $\delta W=0$ is identified as the equilibrium configuration, Fig.S3b. It is observed that as $\gamma/\mu H$ increases, crease

causes less and less deformation on the free surface. Consequently, δW_{surf} becomes negligible during the formation of crease and ε_c approach a constant value for large $\gamma/\mu H$.

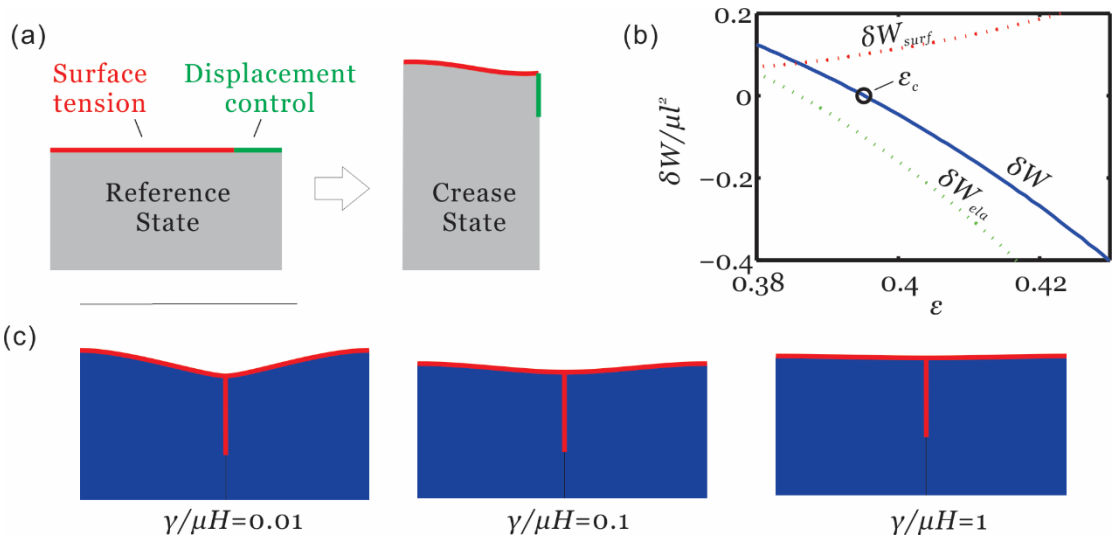

FIG.S3. (a) Schematic of the simulation with fixed contact length. (b) obtain ε for a creased state by comparing the energy difference between a longer crease and a shorter crease. Here $\gamma/\mu H = 0.01$ at plane strain condition. (c) simulation result of the crease tip with different $\gamma/\mu H$.

Generalized plane strain condition

Plane strain condition specifies a deformation where the out of plane deformation is suppressed, Fig.S4a. Generalized plane strain condition specifies a deformation where the out of plane deformation is a uniform stretch, λ_3, Fig.S4b [8]. For a neo-hookean elastomer with constant surface tension γ deforming under plane strain condition (Fig.S4a), the total free energy is:

$$W_{PE} = \int_{bulk} \frac{\mu}{2} F_{\alpha\beta} F_{\alpha\beta} dV + \int_{surface} \gamma \sqrt{F_{11}^2 + F_{12}^2}\, dA + \text{const.} \qquad (32)$$

Here indices $\alpha, \beta = 1, 2$.

(a) Plane strain condition

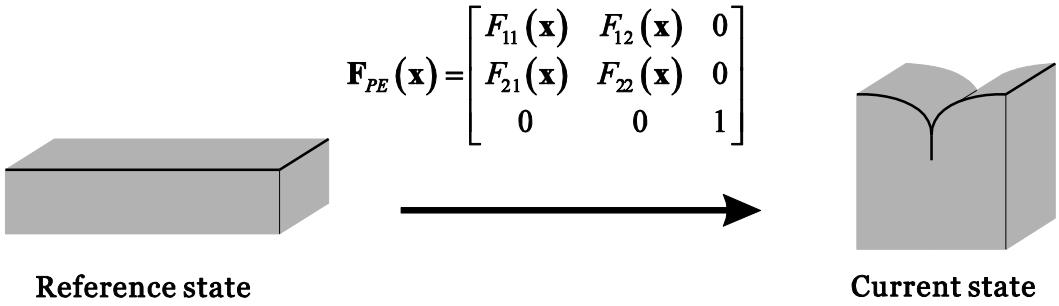

(b) Generalized plane strain condition

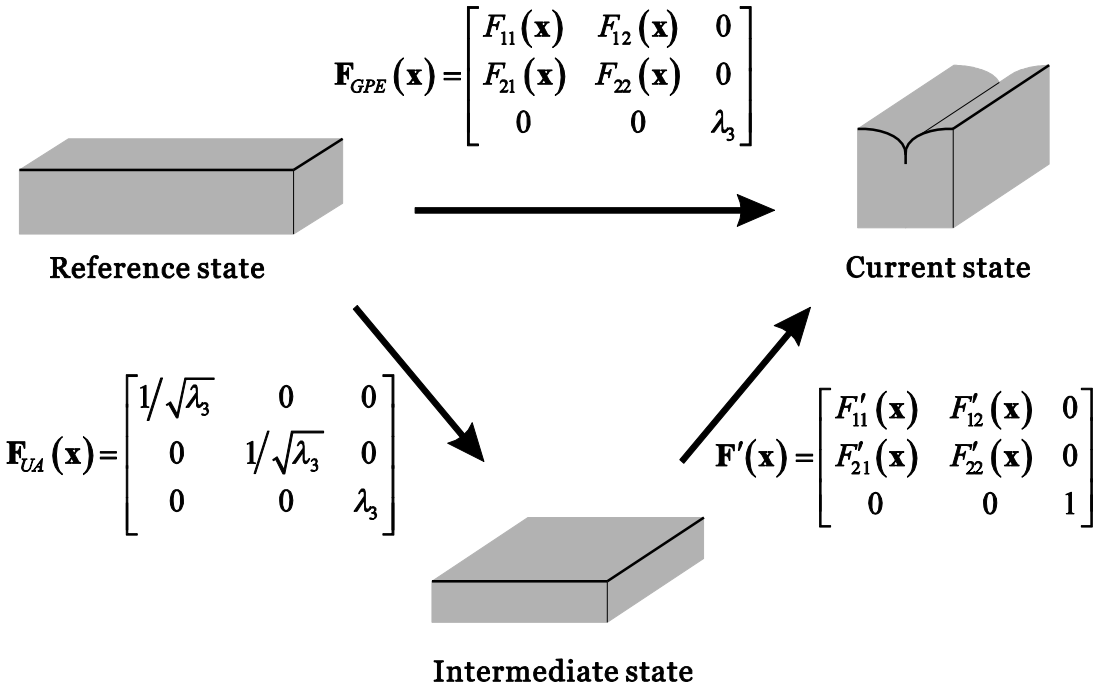

FIG.S4. (a) Plane strain condition. (b) Generalized plane strain condition can be decomposed into a homogeneous uniaxial stretch and a plane strain deformation.

For the same material deforming under generalized plane strain condition, the deformation gradient field can be decomposed into a homogeneous uniaxial stretch $\mathbf{F}_{UA}$ and a plane strain deformation $\mathbf{F}'$, Fig.S4b. The in plane part of $\mathbf{F}'$ is

connected to the overall deformation gradient by the relation:

$$F'_{\alpha\beta} = \sqrt{\lambda_3} F_{\alpha\beta} \tag{33}$$

Write out the total free energy of the material using (33):

$$W_{GPE} = \int_{bulk} \frac{\mu}{2\lambda_3} F'_{\alpha\beta} F'_{\alpha\beta} dV + \int_{surface} \sqrt{\lambda_3}\gamma \sqrt{F'^2_{11} + F'^2_{12}}\, dA + \text{const.} \tag{34}$$

If we take the transformation:

$$\begin{cases} \mu' = \mu/\lambda_3 \\ \gamma' = \gamma\sqrt{\lambda_3} \end{cases} \tag{35}$$

Free energy (34) and (32) takes the same form. This means that thermodynamically a generalized plane strain condition and a plane strain condition are equivalent under the transformation (33) and (35). The corresponding transformation of the crease condition is :

$$\begin{cases} \left(\frac{\gamma}{\mu H}\right)_{PE} = \lambda_3\sqrt{\lambda_3}\frac{\gamma}{\mu H} \\ \lambda_{1PE} = \lambda_1\sqrt{\lambda_3} \end{cases} \tag{36}$$

Experimental verification

The polyurethane (F-105, BJB enterprises) (PU) was used for the mounting layer of the experiments. The choice of a polyurethane elastomer is to provide hydrogen bonding with the gel, providing a level of adhesion that was adequate for our experiments. For a gel of a low modulus, no detachment was observed upon release of the elastomer. For a gel of a high modulus, detachment was observed at high compressive strain; however, within the characterized strain range, there was no

detachment.

F-105A and F-105B were mixed with the ratio of 1:1, followed by degassing until bubbles disappeared. The degassed sample was put at room temperature for 1 hour and then in the oven around 75 °C over 16 h to fully cure it. The PAAm hydrogel was synthesized between a glass slide (25 mm x 75 mm x 1 mm) and the PU mounting later. The glass slide was washed in water, ethanol (PHARMCO-AAPER), and acetone (Fisher Scientific) with sonicator, followed by UVO treatment for 15 min. Then, it was treated with 200 µl (tridecafluoro-1,1,2,2-tetrahydrooctyl)dimethylchlorosilane (Gelest) around 120 °C over 3 days for the clean detachment from the gel. The aqueous pre-gel solution was made with the different concentrations of acrylamide (Sigma-Aldrich) (AAm), bisacrylamide (Research Organics) (BisAAm) and 2.5 v/v% of 3.4 wt% photo initiator VA-086 (Wako Pure Chemical Industries, Ltd.) aqueous solution, and deionized water to tune the shear modulus: from the stiffest sample 7.7 w/v% crosslink 1.9 mol% (AAm 1043 mM and BisAAm 20.2 mM), 5.2 w/v% crosslink 2.9 mol% (AAm 681 mM and BisAAm 19.8 mM), 5.2 w/v% crosslink 0.48 mol% (AAm 718 mM and BisAAm 3.48 mM), 5.2 w/v% crosslink 0.29 mol% (AAm 721 mM and BisAAm 2.10 mM), and 5.2 w/v% crosslink 0.19 mol% (AAm 722 mM and BisAAm 1.40 mM). The shear modulus ranging from ~160 Pa to ~8700 Pa, one and half order difference, was achieved (Fig.S6 and Table S2). The aqueous pre-gel solution was degassed. Then the pre-gel solution was filtered with 0.45 µm pore size filter. After putting the solution inside a glove box filled with nitrogen for 30 min, it was injected between the glass slide and the stretched mounting layer with 1 mm

glass slide spacers in the glove box filled with nitrogen, then exposed by UV light with wavelength of 365 nm for 20 min. To prevent creases nucleating from the edges of the hydrogel due to the instability near the edges during compression, we tuned the sides of the gels by evaporating water from the side edges: although we made hydrogel samples without evaporation during synthesis by controlling humidity in the glove box, the samples mainly showed creases from edges due to the instability near the edges. The evaporation during the synthesis and the pre-strain due to the evaporation were measured (Table S1). The pre-strain was measured by tracking poly(methyl methacrylate) (Mw 350,000, Aldrich) (PMMA) powder particles on the surface of the hydrogel on the PU substrate right after synthesis and these on the surface of the hydrogel detached from the PU substrate then floating on poly(3,3,3-trifluoropropylmethylsiloxane) (Mw 900 – 1000, Gelest).

The compression experiment was conducted with the handmade computer controlled compression machine, the handmade humidity chamber, and a high speed camera setup (Fig.S5). The sample was compressed by releasing the strain of a pre-stretched PU substrate with various kinds of controlled strain and strain rate (0.01 strain/s to 0.3 strain/s, i.e. 1 %strain/s to 30 %strain/s) inside the humidity chamber, where the humidity was controlled around 80 %RH with the humidity chamber in order to minimize evaporation and swelling of the gel during experiments. The weight loss of the gels was less than 3 % during experiments (experimental time is less than 5 min) (Fig.S7). The video image of the surface of hydrogels was taken from the top with a high speed camera, FASTCAM SA3 (Photron), to observe the

surface instability during compression and to measure the critical strain.

For the critical strain analysis, the strains during compression were calculated by measuring the distance between two fixed points of the samples. Either one side or both sides of the crease tips were tracked during the compression, and the critical strain was determined by drawing two linear fitted lines at the early stage of the crease nucleation and growth behavior with the aid of video images and defined as the intersection point of the two linear fitted lines (Fig.S8). At very high strain, buckling of the sample was observed, and the only strain range which satisfies following criteria was analyzed in order to prevent/minimize the effects of the buckling. For the soft gels (shear modulus < 8000 Pa), the measured strain by tracking two makers of the samples ($\varepsilon_{measure}$) is almost the same value as the estimated strain based on the grip distance ($\varepsilon_{estimate} = 1 - l/L$: l and L are the current and the initial length of the PU mounting layer (Fig. S5a and c)) due to the strong modulus mismatch between the hydrogels and the PU mounting layer. Therefore $|\varepsilon_{estimated} - \varepsilon_{measured}| < 0.01$ was used as the criteria. On the other hand, $\varepsilon_{measure}$ of the stiff gel (shear modulus > 8000 Pa) becomes smaller than $\varepsilon_{estimate}$ due to its relatively high stiffness. Only for the stiff gels, $|\varepsilon_{estimated} - \varepsilon_{measured}| < 0.04$ were used as the criteria.

For rheology measurement, the gel was synthesized between two glass slides with a spacer, where a top glass was treated with (tridecafluoro-1,1,2,2-tetrahydrooctyl)dimethylchlorosilane (Gelest) to enhance the detachment of the gel and the bottom glass was treated with

methacryloxyprpyltrichrolosilane (Gelest) to prevent slip from the glass slide. The gel and the bottom glass was attached to the peltier plate of the AR2000, (TA instruments) and the shear modulus of the PAAm hydrogels was measured with an 8 mm stainless parallel-plate at 25 ˚C. The strain between 1 %strain and 5 %strain, which is within a linear regime, was adopted depending on the stiffness of the gels. The storage shear modulus at 1 Hz was adopted (Fig.S6 and Table S2).

The surface tension of each pre-gel solution was measured by the custom made tensiometer. Elastocapillary length (γ/μ) and elastocapillary number ($\gamma/\mu H$) were calculated with the measured shear modulus and surface tension (Table S2).

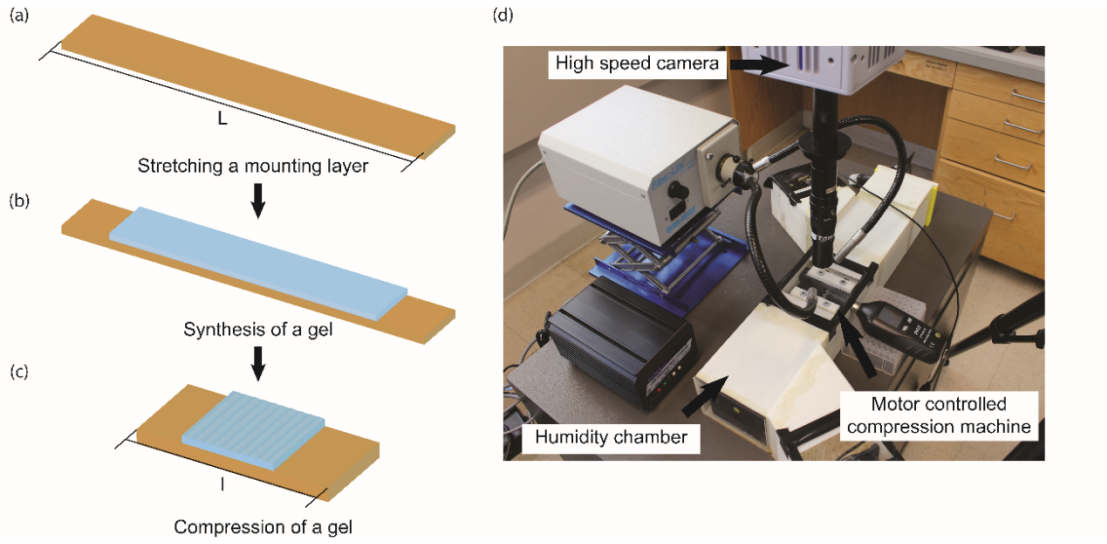

Fig.S5. Experimental setup and procedure: (a) stretching a PU mounting layer, (b) synthesis of PAAm gel on the mounting layer, (c) compressing PAAm gel by releasing strain, and (d) experimental setup of high speed camera, humidity chamber, and motor controlled compression machine.

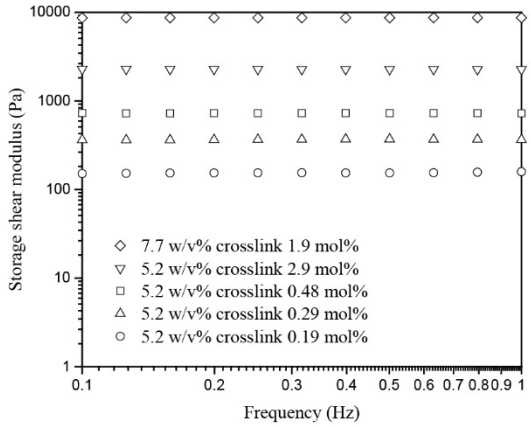

Fig.S6. The rheological measurements of PAAm gel with different concentrations and crosslink densities.

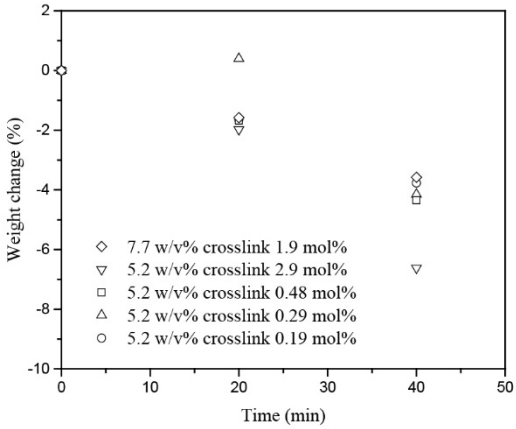

Fig.S7. The weight change of PAAm gels with different concentrations and crosslink densities around 80 %RH.

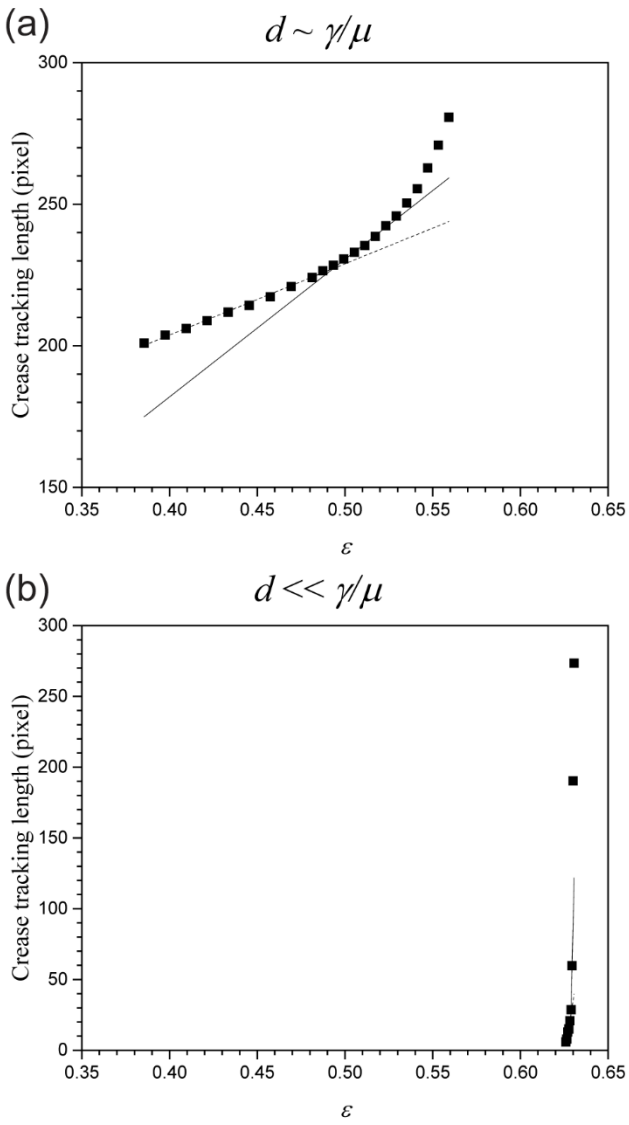

Fig.S8. The crease tracking and the critical strain: (a) sample with visible defects $d \sim \gamma/\mu$ and (b) sample without visible defects $d << \gamma/\mu$.

Table S1. Weight loss during synthesis and resulting pre-strain

PAAm gel concentration	7.7 w/v% crosslink 1.9 mol%	5.2 w/v% crosslink 2.9 mol%	5.2 w/v% crosslink 0.48 mol%	5.2 w/v% crosslink 0.29 mol%	5.2 w/v% crosslink 0.19 mol%
Weight loss during synthesis (wt%)	16.2	15.8	16.7	14.6	17.3
Pre-elongation strain ε_x	0.066±0.002	0.070±0.007	0.080±0.003	0.083±0.003	0.082±0.003
Pre-elongation strain ε_y	0.006±0.004	0.006±0.001	0.017±0.006	0.014±0.009	0.019±0.005

Table S2. Shear modulus, surface tension, elastocapillary number, and elastocapillary length

PAAm gel concentration	7.7 w/v% crosslink 1.9 mol%	5.2 w/v% crosslink 2.9 mol%	5.2 w/v% crosslink 0.48 mol%	5.2 w/v% crosslink 0.29 mol%	5.2 w/v% crosslink 0.19 mol%
Shear modulus (Pa)	8700	2300	720	370	160
Surface tension (mN/m)	63	65	65	65	65
Elastocapillary length (mm)	0.0073	0.029	0.091	0.18	0.41
Elastocapillary number	0.0073	0.029	0.091	0.18	0.41

Video S1. The PAAm hydrogel with $\gamma/\mu = 0.091$ mm: a few creases nucleate from the defects of $d \sim \gamma/\mu$ and some creases appeared homogeneously near $\varepsilon_{wrinkle}$ (strain rate is 0.15 strain/s). Play speed is 0.13x.

Video S2. The PAAm hydrogel with high $\gamma/\mu = 0.091$ mm: many creases appeared homogeneously near $\varepsilon_{wrinkle}$ (strain rate is 0.15strain/s). Play speed is 0.13x.

1. Style, R.W., et al., *Elastocapillarity: Surface tension and the mechanics of soft solids*. Annual Review of Condensed Matter Physics, 2017. **8**: p. 99-118.
2. Rubinstein, M. and R. Colby, *Polymers physics*. Vol. 767. 2003: Oxford Oxford, UK.
3. Flory, P.J. and J. Rehner Jr, *Statistical Mechanics of Cross-Linked Polymer Networks I. Rubberlike Elasticity*. The Journal of Chemical Physics, 1943. **11**(11): p. 512-520.
4. Flory, P.J. and J. Rehner Jr, *Statistical mechanics of cross-linked polymer networks II. Swelling*. The Journal of Chemical Physics, 1943. **11**(11): p. 521-526.
5. Zhao, X., W. Hong, and Z. Suo, *Electromechanical hysteresis and coexistent states in dielectric elastomers*. Physical review B, 2007. **76**(13): p. 134113.
6. Mora, S., et al., *Surface instability of soft solids under strain*. Soft Matter, 2011. **7**(22): p. 10612-10619.

7. Riks, E., *The application of Newton's method to the problem of elastic stability*. Journal of Applied Mechanics, 1972. **39**(4): p. 1060-1065.
8. Hong, W., X. Zhao, and Z. Suo, *Formation of creases on the surfaces of elastomers and gels*. Applied Physics Letters, 2009. **95**(11): p. 111901.